PROCEEDINGS OF SPIE

SPIEDigitalLibrary.org/conference-proceedings-of-spie

Contribution of scatter and beam hardening to phase contrast imaging

Cale Lewis, Ivan Vazquez, Stefano Vespucci, Mini Das

Cale Lewis, Ivan Vazquez, Stefano Vespucci, Mini Das, "Contribution of scatter and beam hardening to phase contrast imaging," Proc. SPIE 10948, Medical Imaging 2019: Physics of Medical Imaging, 109485G (13 March 2019); doi: 10.1117/12.2513512



Event: SPIE Medical Imaging, 2019, San Diego, California, United States

Contribution of Scatter and Beam Hardening to Phase Contrast Imaging

Cale Lewis^a, Ivan Vazquez^a, Stefano Vespucci^a, and Mini Das^{a,b}

^aDepartment of Physics ^bDepartment of Biomedical Engineering University of Houston, Houston, TX 77204

ABSTRACT

X-ray phase contrast imaging is being investigated with the goal of improving the contrast of soft tissue. Enhanced edges at material boundaries are characteristic of phase contrast images. These allow better retrieval of phase maps and attenuation maps when material properties are very close to each other. Previous observations have shown that the edge contrast of a target material reduces with increasing thickness of the surrounding bulk material. In order to accurately retrieve material properties, it is important to understand the contributions from various factors that may lead to this phase degradation. We investigate this edge degradation dependence due to beam hardening and object scatter that results from the surrounding bulk material. Our results suggest that the large propagation distances used in PB-PCI are effective at reducing the scatter influence. Rather, our results indicate that the phase contrast degradation due to beam hardening is the most critical. The ability to account for these variations may be necessary for more accurate phase retrievals using polychromatic sources and large objects.

Keywords: X-ray, Medipix, Phase Contrast Imaging

1. INTRODUCTION

The complementary absorption and transmission rates of x-rays through matter is fundamental to conventional x-ray imaging, where applications can be found in security and medicine. Such absorption-based x-ray imaging techniques rely on distinct absorption properties to distinguish the different underlying materials. However, this approach can be limited for discriminating biological tissues with similar absorption properties.

More recently, techniques are being developed to measure the phase signal of x-rays that have traversed through a medium. This approach relies on the mediums index of refraction:¹

$$n = 1 - \delta + i\beta,\tag{1}$$

where $\delta = \frac{r_e \lambda^2}{2\pi} \rho_e$ is the phase decrement that depends on the photon wavelength λ and the medium's electron density ρ_e , while the complex part β is related to the x-ray absorption. For biological tissue, δ is many magnitude larger than β , which means larger phase signal is expected than absorption.

There are many techniques being developed to measure the phase signal of the traversed x-rays. One of the main requirements are for the incident beam to have high coherence. One approach grating interferometers which applies absorbing grids to generate a series of periodic psuedo-sources.³ A similar method known as coded aperture⁴ has been developed which relaxes some of the restrictions on grating interferometers by reducing the need for translational scanning. However, both of these approaches rely on including gridded structures to the beam path which require high precision and also increases the exposure to the patient.

Recent advancements in micro-focus x-ray source technology have made available sources with relatively high coherence. These micro-focus sources can be used to generate a high coherence beam such that the phase signal can be obtained by increasing the propagation distance from the object and detector.⁵ This propagation-based

Author for correspondence: Mini Das: E-mail: mdas@uh.edu

Medical Imaging 2019: Physics of Medical Imaging, edited by Taly Gilat Schmidt, Guang-Hong Chen, Hilde Bosmans, Proc. of SPIE Vol. 10948, 109485G · © 2019 SPIE · CCC code: 1605-7422/19/\$18 · doi: 10.1117/12.2513512

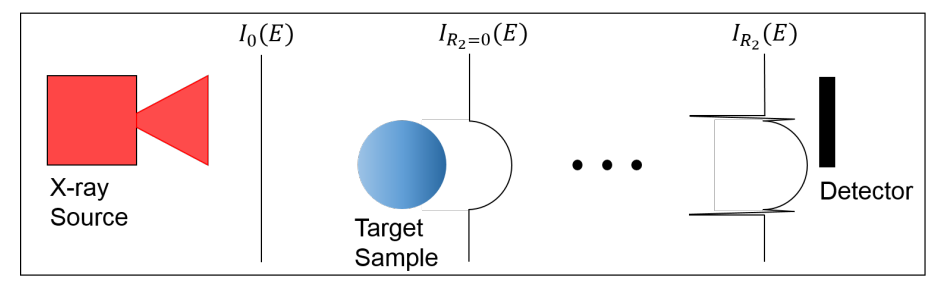


Figure 1: Schematic of the PB-PCI set-up which requires a micro-focus x-ray source and long propagation distances to produce the edge enhancement.

phase contrast (PB-PCI) imaging modality requires no additional components to the beam path. The intensity measured at the detector plane in a PB-PCI set-up can be described by the following transport-of-intensity (TIE) equation:⁶

$$I_R(E) = \frac{I_0(E)}{M^2} \cdot \exp\left(-\int \mu(E)dl - \frac{R_2}{Mk(E)} \nabla^2 \phi(E)\right),\tag{2}$$

where $I_0(E)$ is the incident spectrum, M is the magnification, $\int \mu(E)dl$ is the integrated attenuation coefficient over the x-ray path, R_2 is the distance from the object plane to the detector plane, ∇^2 is the spatial Laplacian on the x-ray phase $\phi(E) = -\frac{2\pi}{\lambda} \int \delta(l)dl$ with wavenumber $k(E) = \frac{2\pi E}{hc}$. Replacing the ϕ leads to:

$$\frac{I_R(E)}{I_0(E)} = M^{-2} \cdot \exp\left(-\int (\mu(E) + \frac{(hc)^2 r_e R_2}{M2\pi E^2} \nabla^2 \rho_e) dl\right). \tag{3}$$

An illustration of the intensity varying with the propagation distance is shown in Figure 1. Sharp discontinuities of the electron density result in enhanced edge signals which are characteristic of PB-PCI. The enhanced edges allow better retrieval of phase maps and attenuation maps when material properties are very close to each other.

Our recent observations⁷ have shown that edge contrast of a target material reduces with increasing thickness of the surrounding bulk material. This is problematic since clinical applications desire finding targets that are embedded in a larger bulk. In order to accurately retrieve material properties, it is important to understand the contributions from various factors that may lead to this phase degradation. We investigate this edge degradation dependence due to beam hardening and object scatter that is caused by the surrounding bulk material.

The main goal of this paper is to determine the contributions to the edge contrast degradation with various benchtop parameters. In particular, we would like to provide more insight to the issue of edge contrast reduction with increasing bulk around the target material. Typical reasons for contrast reduction include object scatter, beam hardening, and an increase to the effective energy. Of these, we would like to determine which factor is the most prominent in reducing the edge contrast.

2. METHODS

2.1 Experiment Bench Top

An experimental set-up was prepared to investigate the influence of an additional bulk material on the edge enhancement of the target material. The edge-illumination in this study is obtained using a free-space phase contrast geometry. This set-up requires a small focal spot x-ray source and sufficiently large propagation distances between the components.

A tungsten anode Hamamatsu L8121-03 micro-focus x-ray tube was used to generate a polychromatic spectrum with a 7 um focal spot size. The source has an inherint 200 um beryllium output window, and no additional filtering was included. The source beam was incident on a 6.2 mm diameter PMMA rod that was fixed at a distance of 57 cm. A Medipix3RX photon counting detector used as the image receptor which was placed 136 cm from the target.

The Medipix3RX detector consists of a 256×256 pixel array with 55 um pitch with a direct conversion semiconductor sensor. A 1000 um thick CdTe sensor was used in our study. While the Medipix3RX has energy-resolving capabilities, the detector was operated with a single threshold energy such that all incident photons above 8.5 keV were recorded. Additionally, the Medipix3RX detector was operated in 'charge-summing mode'9 to reduce the spectral distortions due to charge-sharing effects. Temporal distortions were minimized by resetting the -500 V bias in between each measurement.

For each projection, an image profile was obtained by averaging the intensities along the vertical direction. The edge contrast with the background intensity was used to quantify the changes to the edge enhancement. The edge contrast was calculated by,

$$C_{edge} = \frac{I_{edge} - I_{bg}}{I_{bg}},\tag{4}$$

where I_{edge} is the maximum intensity of the image profile and I_{bg} is the mean of the image profile taken from a region where the rod was not present.

2.1.1 Varying Bulk Thickness and Position

In practical applications, the target is likely to be surrounded by additional bulk material. We have used PMMA slabs of varying thickness to observe the change in the visibility of the target edge. The average lateral dimensions of the slabs were 15.0×10.2 cm² and were fully exposed by the source beam. In a practical setting, the target would be embedded in the bulk. Our study instead added additional bulk slabs to the path and any edge enhancement was due to the boundary between the air and target rod.

In addition to varying the thickness, the bulk position was also changed. Initially, the additional bulk was placed closely at a distance 1.5 cm after the target rod. This bulk-to-detector distance provides a decent estimate for a practical sample in PB-PCI. The influence of the bulk scatter was investigated by moving the bulk 2 cm before the detector. The reduced bulk-to-detector distance increases the angle subtended by the detector and therefore increases the amount of scatter collected.

2.1.2 Varying Tube Potential

The contrast is expected to also reduce with increased incident energy. This was investigated by removing the PMMA bulk slabs and instead varying the tube potential. The x-ray source has power limitations that prevent high flux operation. Further, the maximum current setting reduces as the tube potential is increased. We sought to maximize the flux from the source and therefore the maximum current was used for each applied tube potential.

2.2 Simulation Procedure

An analytic simulation has been prepared in Matlab based on the PB-PCI TIE decribed in Equation 3. An incident spectrum based on the desired tube potnential is modeled using the Spektr toolkit. 10,11 Attenuation and δ projections 12 were obtained by defining the sample geometry and material properties. 13,14 The TIE is then applied across the projections for each energy to obtain the intensity at the detector. The absorption efficiency of a 1000 um thick CdTe detector was modeled based on the known sensor thickness and attenuation. Other detector effects such as charge-sharing and fluorescence were not included.

3. RESULTS AND DISCUSSIONS

3.1 Varying the Bulk Thickness and Position

Edge enhancement of the sample rod occurs in the PB-PCI set-up due to the transition from the air to the PMMA, as demonstrated in Figure 2a. The edge signal is complimentary to the absorption contrast for improving structure identification. Both the image contrast and edge visibility reduces when including additional PMMA bulk slabs, as shown in Figure 2b. The corresponding image profiles in Figure 2c and 2d show an edge contrast of 12.3% and 8.5% for the rod-only and rod+bulk, respectively.

Previous observations have shown that the edge contrast reduces with increased thickness of the bulk slabs. We conducted an investigation to evaluate the influence of the scatter signal from the additional bulk material

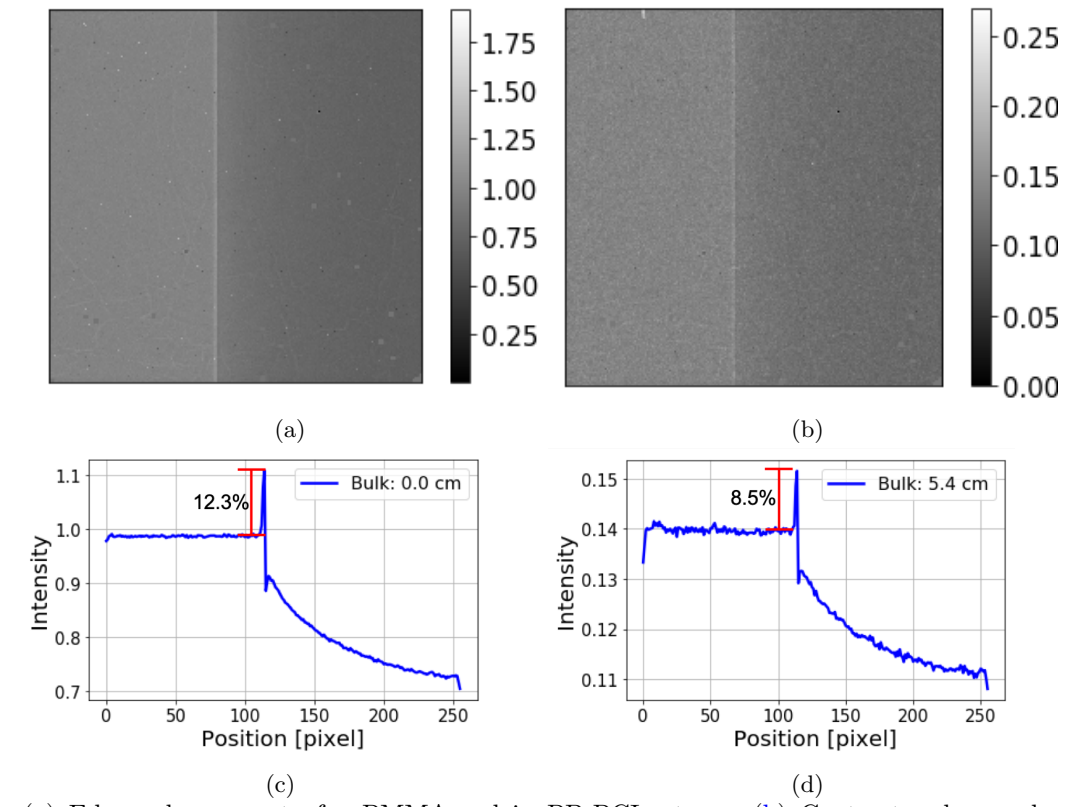


Figure 2: (a) Edge enhancement of a PMMA rod in PB-PCI set-up. (b) Contrast reduces when including additional 5.2 cm thick surrounding bulk material placed after the sample. (c-d) Image profiles obtained by taking the mean along the vertical direction shows a 3.8% edge contrast reduction between rod-only and rod+bulk images, respectively. The incident spectrum was generated with a 40 keV peak voltage.

on the edge contrast reduction. Positioning the bulk material near the detector reduces the air gap and increases the scatter signal which results in additional contrast loss, as shown in Figure 3.

However, the edge contrast values obtained when the bulk was located near the target show a reasonable match with the simulation values. This suggests that the scatter signal from the bulk surrounding the target rod is negligible to the edge contrast reduction. This is not surprising considering the large propagation distances of the PB-PCI set-up are an effective scatter rejection technique. Therefore, the edge contrast reduction with bulk thickness is most likely due to the beam hardening.

3.2 Varying the Tube Potential

The results of the previous section have suggested that the edge contrast reduces with increasing bulk thickness due to beam hardening. Therefore, the influence of the incident energy was investigated by varying the tube potential. The edge contrast is expected to decrease with increasing incident energy as predicted by Equation 3, which is shown in Figure 4. Further agreement is observed between the experiment and simulation edge contrast. The differences, which occur more at the lower tube potentials, are likely due to the non-ideal detector response including fluorescence and charge-sharing in the experiment.

The mean energy of the spectral distributions for varying the tube potential and bulk thickness were obtained. Therefore, the edge contrast reduction for each parameter can be compared as a function of the effective energy, as shown in Figure 5. The edge contrast reduces more rapidly with increasing bulk thickness although the same effective energy can be obtained with a different tube potential. This occurs because the effective energy for the increasing bulk thickness is due to a filtering off of the low energy photons. Alternatively, increasing the tube

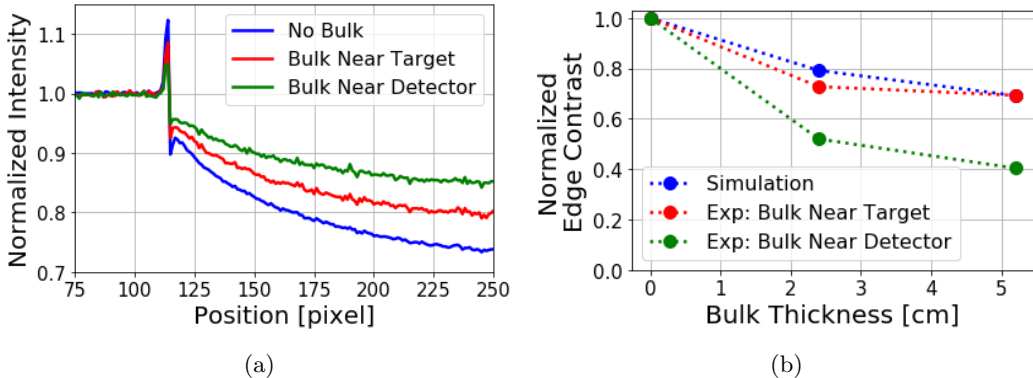


Figure 3: (a) The contrast reduces more severely when the 5.2 cm thick additional bulk slab is placed near the detector surface due to the increased scatter-to-primary ratio. (b) The rate at which the contrast reduces with increasing bulk thickness is similar for when it is positioned near the target and the simulation prediction.

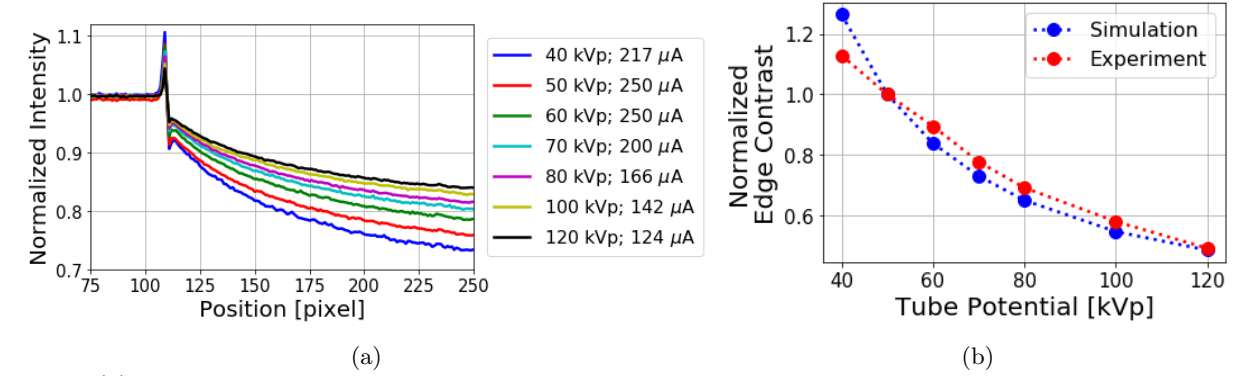


Figure 4: (a) Contrast reduces with increasing tube potential due to the increased effective energy of the incident beam. (b) A decent match for the contrast reduction is observed between the experiment and simulation when normalized to the contrast at 50 kVp.

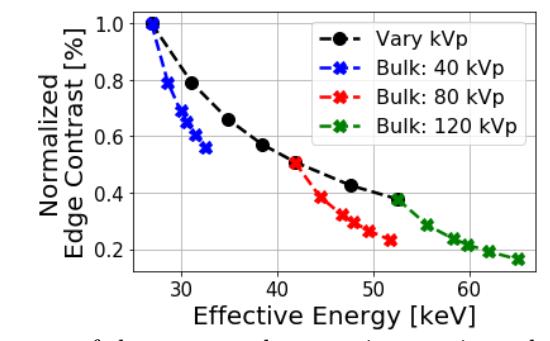


Figure 5: Simulated edge contrast of the target rod comparing varying tube potential and bulk thickness.

potential preserves these low energy photons. According to Equation 3, these low energy photons provide more contrast.

4. CONCLUSIONS

The contributions to the contrast degradation of the edge-illumination in phase contrast imaging due to a bulk material have been investigated. The edge contrast of a target sample reduces for increasing bulk thickness. Both beam hardening and object scatter due to the bulk have been considered.

Our results suggest that the influence of the scatter is negligible when the bulk is placed near the target due to the large propagation distances in PB-PCI geometry. The edge contrast obtained with the experimental set-up for varying bulk thickness closely resembled the trends observed with the simulation. Reducing the bulk-to-detector distance caused a noticeable decrease to the edge contrast, but this would not occur in a practical measurement.

The remaining effect that reduces the edge contrast is the beam hardening of the bulk material. Comparisons of the edge contrast were made between the varying bulk thickness and varying tube potential. The filtering of the low energy photons due to beam hardening were shown to have a greater influence in reducing the edge contrast than for varying the tube potential. Overall, the edge signal remains visible for a bulk thickness of 5.2 cm, suggesting potential applications in small animal or breast imaging.

ACKNOWLEDGMENTS

This work was partially supported by funding from the US Department of Defense (DOD) Congressionally Directed Medical Research Program (CDMRP) Breakthrough Award BC151607 and the National Science Foundation CAREER Award 1652892.

REFERENCES

- [1] Als-Nielsen, J. and McMorrow, D., [Elements of modern X-ray physics], John Wiley & Sons (2011).
- [2] Lewis, R., "Medical phase contrast x-ray imaging: current status and future prospects," *Physics in medicine* & biology **49**(16), 3573 (2004).
- [3] Pfeiffer, F., Weitkamp, T., Bunk, O., and David, C., "Phase retrieval and differential phase-contrast imaging with low-brilliance x-ray sources," *Nature physics* **2**(4), 258 (2006).
- [4] Olivo, A. and Speller, R., "A coded-aperture technique allowing x-ray phase contrast imaging with conventional sources," *Applied Physics Letters* **91**(7), 074106 (2007).
- [5] Wilkins, S., Gureyev, T. E., Gao, D., Pogany, A., and Stevenson, A., "Phase-contrast imaging using poly-chromatic hard x-rays," *Nature* **384**(6607), 335 (1996).
- [6] Gürsoy, D. and Das, M., "Single-step absorption and phase retrieval with polychromatic x rays using a spectral detector," *Optics letters* **38**(9), 1461–1463 (2013).
- [7] Vespucci, S., Lewis, C., Park, C. S., and Das, M., "Examining phase contrast sensitivity to signal location and tissue thickness in breast imaging," in [Medical Imaging 2018: Physics of Medical Imaging], 10573, 1057324, International Society for Optics and Photonics (2018).
- [8] Siewerdsen, J. H. and Jaffray, D. A., "Cone-beam computed tomography with a flat-panel imager: Magnitude and effects of x-ray scatter," *Medical physics* **28**(2), 220–231 (2001).
- [9] Ballabriga, R., Alozy, J., Blaj, G., Campbell, M., Fiederle, M., Frojdh, E., Heijne, E., Llopart, X., Pichotka, M., Procz, S., et al., "The Medipix3RX: a high resolution, zero dead-time pixel detector readout chip allowing spectroscopic imaging," *Journal of Instrumentation* 8(02), C02016 (2013).
- [10] Siewerdsen, J., Waese, A., Moseley, D., Richard, S., and Jaffray, D., "Spektr: A computational tool for x-ray spectral analysis and imaging system optimization," *Medical physics* **31**(11), 3057–3067 (2004).
- [11] Boone, J. M. and Seibert, J. A., "An accurate method for computer-generating tungsten anode x-ray spectra from 30 to 140 kv," *Medical physics* **24**(11), 1661–1670 (1997).
- [12] Siddon, R. L., "Fast calculation of the exact radiological path for a three-dimensional ct array," *Medical physics* **12**(2), 252–255 (1985).
- [13] Torikoshi, M., Tsunoo, T., Sasaki, M., Endo, M., Noda, Y., Ohno, Y., Kohno, T., Hyodo, K., Uesugi, K., and Yagi, N., "Electron density measurement with dual-energy x-ray ct using synchrotron radiation," *Physics in Medicine & Biology* 48(5), 673 (2003).
- [14] White, D., Booz, J., Griffith, R., Spokas, J., and Wilson, I., "Tissue substitutes in radiation dosimetry and measurement, the international commission on radiation units and measurements (icru), report 44," (1989).
- [15] Davis, T., Gao, D., Gureyev, T., Stevenson, A., and Wilkins, S., "Phase-contrast imaging of weakly absorbing materials using hard x-rays," *Nature* **373**(6515), 595 (1995).
- [16] Paganin, D., [Coherent X-ray optics], no. 6, Oxford University Press on Demand (2006).

- [17] Teague, M. R., "Deterministic phase retrieval: a greens function solution," JOSA 73(11), 1434–1441 (1983).
- [18] Del Sordo, S., Abbene, L., Caroli, E., Mancini, A. M., Zappettini, A., and Ubertini, P., "Progress in the development of CdTe and CdZnTe semiconductor radiation detectors for astrophysical and medical applications," Sensors 9(5), 3491–3526 (2009).